SCIENCE CHINA Materials ARTICLES

mater.scichina.com link.springer.com

Published online 27 September 2017 | doi: 10.1007/s40843-017-9097-8
Sci China Mater 2017, 60(10): 955–962

Rational synthesis of SnS_2@C hollow microspheres with superior stability for lithium-ion batteries

Hulin Yang[1†], Yanhui Su[1†], Lin Ding[1], Jiande Lin[1], Ting Zhu[1*], Shuquan Liang[1], Anqiang Pan[1*] and Guozhong Cao[2]

ABSTRACT **Tin-based nanomaterials have been extensively explored as high-capacity anode materials for lithium ion batteries (LIBs). However, the large volume changes upon repeated cycling always cause the pulverization of the electrode materials. Herein, we report the fabrication of uniform SnS_2@C hollow microspheres from hydrothermally prepared SnO_2@C hollow microspheres by a solid-state sulfurization process. The as-prepared hollow SnS_2@C microspheres with unique carbon shell, as electrodes in LIBs, exhibit high reversible capacity of 814 mA h g^{-1} at a current density of 100 mA g^{-1}, good cycling performance (783 mA h g^{-1} for 200 cycles maintained with an average degradation rate of 0.02% per cycle) and remarkable rate capability (reversible capabilities of 433 mA h g^{-1} at 2 C). The hollow space could serve as extra space for volume expansion during the charge-discharge cycling, while the carbon shell can ensure the structural integrity of the microspheres. The preeminent electrochemical performances of the SnS_2@C electrodes demonstrate their promising application as anode materials in the next-generation LIBs.**

Keywords: tin disulfide, hollow microspheres, lithium-ion battery, anode material, carbon coating

INTRODUCTION

As one of the most successful power sources, lithium ion batteries (LIBs) have dominated the power market of high-tech electronic devices and electrical vehicles due to their high energy density [1–3]. However, the ever-increasing requirements from the customers stimulate the continuous efforts to develop advanced electrode materials with high energy density, good stability, low-cost and good safety [4]. The relatively low storage capacity of commercial graphite anode (372 mA h g^{-1}) cannot meet the high energy density requirement for the next-generation LIBs [5]. To address this issue, tin and tin-based materials (such as SnO, SnO_2, and SnS_2) have been extensively studied as the alternative anodes owing to their low operating voltage, high theoretical capacities and low cost [6–9]. Among them, SnS_2 has been suggested as a promising candidate for LIBs anodes because of its CdI_2-type layered structure, in which the tin atoms are sandwiched between two layers of hexagonally close-packed sulfur atoms. The neighboring sulfur layers bonded by the weak Van der Waals interactions facilitate kinetically for Li^+ insertion and extraction [10,11]. This space among the layers, as a host for insertion and extraction of Li^+ [12,13], contributes to a high theoretical capacity. Compared with the tetragonal rutile SnO_2, the CdI_2-type layered structure of SnS_2 is more favorable for the cycle performance of electrode, because the layers with weak interaction are more flexible for repeated insertion and extraction of ions. Moreover, the Li_2S, produced by the irreversible reaction of SnS_2 and Li^+, can serve as a buffer in Li-Sn alloying-dealloying process. Unfortunately, the intrinsically low electrical conductivity and extremely large volume change (approximate 300% during lithiation and delithiation) lead to capacity decay, commonly reported for tin-based anode materials [14], and poison the electrochemical performance of SnS_2 electrode materials [15].

Many efforts have been endeavored to make nanostructured SnS_2 or their composites. Because rational morphological design of active materials can relieve internal stress caused by volumetric expansion and thus protect the microstructure from collapse during the diffusion of ions. Moreover, minimizing particle sizes can shorten the diffusion distance of lithium ions and the electronic transportation distance [16,17]. To date, var-

[1] School of Materials Science and Engineering, Central South University, Changsha 410083, China
[2] Department of Materials Science & Engineering, University of Washington, Seattle, WA 98195, USA
[†] These authors contributed equally to this work.
[*] Corresponding authors (emails: zhut0002@csu.edu.cn (Zhu T); pananqiang@csu.edu.cn (Pan A))

ious SnS_2 hierarchical microstructures with different morphologies, such as microflowers [18], microspheres [19], microplates [10] and microbelts [20], were synthesized to improve the electrochemical properties. Furthermore, carbon materials are introduced into SnS_2 microstructures as the conductive agent to increase the electrical conductivity of the electrode materials [21,22]. For example, Kong *et al.* [23] fabricated free-standing SnS_2@graphene microcables, with a stable specific capacity of 720 mA h g^{-1} at a current density of 0.2 A g^{-1}. Liu *et al.* [24] reported a 3D free-standing SnS_2 with polypyrrole-microbelt and carbon-microtube, which showed a capacity of 757 mA h g^{-1} at a current density of 1 C. Based on the above reported work, a speculation can be made that carbon structures can enhance the physical property by serving as conductive agents, ion channel and volume expansion buffer in the SnS_2@C structure. So, it would be feasible to design a sophisticated SnS_2/C composite, which provides enough space for the volume extraction and contraction of SnS_2 and good contact between the active material and carbon.

Herein, we successfully constructed carbon-coated SnS_2 hollow microspheres by a sulfurization of carbon coated SnO_2 hollow spheres. In this case, the hollow structures and protective carbon shells can effectively buffer the volumetric expansion of inner SnS_2 electroactive materials as well as preserve the structural integrity of the whole structures [25,26]. As illustrated in Scheme 1, the detailed formation process of the SnS_2@C hollow microspheres involves three steps. In the presence of urea and potassium stannate in an ethanol solution, SnO_2 hollow microspheres were fabricated by a facile hydrothermal method (step I). The as-synthesized SnO_2 hollow microspheres were then uniformly coated with glucose-derived carbon species in a subsequent hydrothermal process to generate SnO_2@C core-shell structures (step II). In sulfurization process (step III, the last step), the as-formed SnO_2@C core-shell structures were mixed with thiourea as a sulfur source and annealed in a vacuum atmosphere to obtain SnS_2@C hollow microspheres. The core-shell SnS_2@C exhibit good electrochemical properties as anode materials for lithium ion batteries.

EXPERIMENTAL SECTION

Synthesis of SnO_2 hollow microspheres

In a typical synthesis, $K_2SnO_3{\cdot}H_2O$ (0.384 g) and urea (0.96 g) were dissolved into 80 mL of mixed solution (50 mL distilled water and 30 mL ethanol) under moderate stirring for 5 min, and a white translucent suspension was obtained. Then the suspension was transferred into a Teflon-lined autoclave and heated at 190°C for 15 h. After the solution was cooled down naturally, the white product was collected by centrifugation and washed with ethanol and water for six times before dried at 50°C overnight in a vacuum oven.

Synthesis of SnS_2 hollow microspheres

Carbon coating of SnO_2 hollow microspheres was conducted by a facile hydrothermal treatment. In a typical procedure, 0.15 g of the as-synthesized SnO_2 powder and 0.6 g glucose were added to a mixture of distilled water and ethanol before stirring for 10 min. The mixture was hydrothermally treated at 190°C for 10 h and cooled down naturally. The brown product was collected by centrifugation and washed with ethanol for six times before dried at 50°C in a vacuum oven for 12 h. Finally, the as-obtained SnO_2@C powder was sulfurized in a vacuum atmosphere at 350°C for 12 h by the introduction of thiourea during the heat treatment.

Electrochemical measurements

The as-prepared SnS_2@C microspheres, acetylene black and polyvinylidene fluoride (PVDF) binder (with a weight ratio of 8:1:1) were stirred with a solution of *N*-methyl-2-pyrrolidone (NMP) to form a homogeneous slurry. The well-mixed slurry was then coated onto a copper foil and dried at 90°C overnight in a vacuum oven

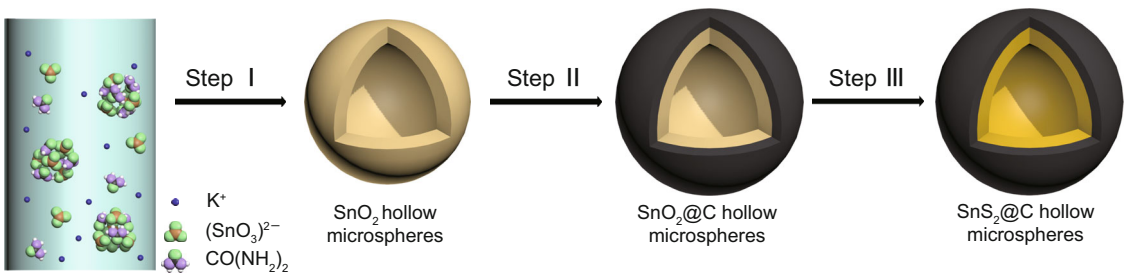

Scheme 1 Schematic illustration of the formation of SnS_2@C hollow microspheres.

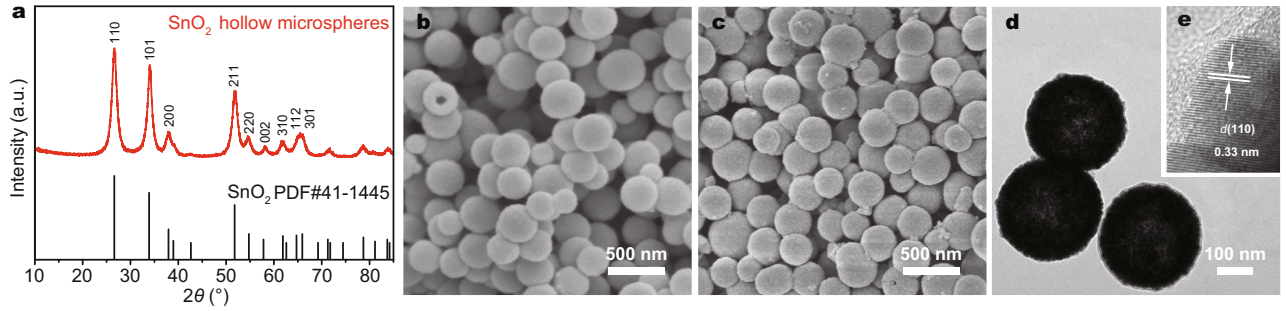

Figure 1 Characterizations of the precursors. (a) XRD pattern of the SnO_2; (b) SEM of the SnO_2; (c) SEM of the SnO_2@C; TEM (d) and HR-TEM (e) images of the SnO_2@C.

to obtain the anodes with a diameter of 12 mm. Coin cells were assembled in an ultra-high purity argon-filled glove box (Mbraun, Germany) using microporous polypropylene membrane as a separator, Li metal foil as the counter electrode and 1 mol L^{-1} $LiPF_6$ (dissolved in ethylene carbonate/dimethylcarbonate/diethyl carbonate, EC/DMC/DEC=1:1:1 in volume) as the electrolyte. The charge-discharge performances between 0.01 to 3 V (*vs.* Li/Li^+) of the cells were recorded in Land Battery Tester (Land CT 2001A, Wuhan, China). Cyclic voltammetry (CV) was carried out using an electrochemical workstation (CHI660C, China) in a voltage range of 0.01–3 V (*vs.* Li/Li^+) at a scan rate of 0.05 mV s^{-1}.

RESULTS AND DISCUSSION

The crystallographic structures of the precursors were first examined by the X-ray diffraction (XRD) and the results are shown in Fig. 1a. The XRD pattern of the SnO_2 hollow microspheres can be assigned to tetragonal phase of SnO_2 (JCPDS No.41-1445, $p42/mnm$ (136), $a=b$ =4.738 Å, c=3.187 Å). Fig. 1b shows the scanning electron microscopy (SEM) images of the SnO_2 hollow microspheres, which have good uniformity with an average diameter of 300 nm. The formation of the SnO_2 hollow microspheres can be explained by an inside-out Ostwald ripening mechanism. The white translucent suspension is produced by the hydrolysis of stannate. The inside-out ripening causes the dissolution of inner part of precipitation and finally results in the hollow interiors during hydrothermal process [6]. From the SEM image of SnO_2@C shown in Fig. 1c, a rough surface of the spheres can be observed. Meanwhile, no obvious morphological and structural changes can be found after carbon-coating, revealing the structural robustness of the spheres. The interior structure of the SnO_2@C microspheres were investigated by transmission electron microscopy (TEM) and high-resolution TEM (HRTEM). As shown in Fig. 1d, e, the periphery of microspheres shows a distinct contrast to the central part, indicating hollow interior of the spheres. The lattice fringes shown in a HRTEM image (Fig. 2d) indicate a good crystallinity with an interplanar distance of 0.33 nm, which is in good accordance with the d-spacing values of tetragonal SnO_2 (110). The amorphous carbon coating layer is clearly observed on the surface of the SnO_2 hollow microspheres [6,8].

After sulfurization with thiourea in vacuum, the SnO_2@C hollow microspheres were transformed into SnS_2@C hollow microspheres. The crystal phase of the SnS_2@C can be confirmed by the presence of the XRD peaks (Fig. 2a), consistent with the hexagonal SnS_2 phase (JCPDS No. 83-1705, p-3m1(164), $a=b$=3.638 Å, c =5.880 Å). Raman testing of the SnS_2@C provided the evidence for the existence of carbon in the final products (Fig. 2b). Raman peaks that appear at the wave number around 1350 and 1580 cm^{-1} can be assigned to the D-band and G-band of carbon species, respectively [27]. Specifically, G-band represents the graphitic feature, while D-band signifies the disorder degree of carbon caused by the existence of tiny crystalline grains [28]. The thermal gravimetric analysis (TGA) and differential thermal analysis (DTA) were operated on the SnS_2@C sample, and the curves are shown in Fig. 2c. The peak of DTA curve at about 450°C corresponds to the oxidation of SnS_2, and the carbon in sample began to burn at 500°C. According to the weight change of TGA curve, the content of carbon in the SnS_2@C is about 14%. The SEM image of SnS_2@C (Fig. 2d) shows no distinct structural changes after sulfurization compared to the SnO_2 and SnO_2@C microspheres, indicating the good structural reservation of the carbon coated SnS_2 spheres. Fig. 2e shows the TEM image of SnO_2@C microspheres, indicating a hollow interior of the microsphere. An HR-TEM image (Fig. 2f) further elucidates that the SnS_2 microspheres were coated by amorphous carbon with an

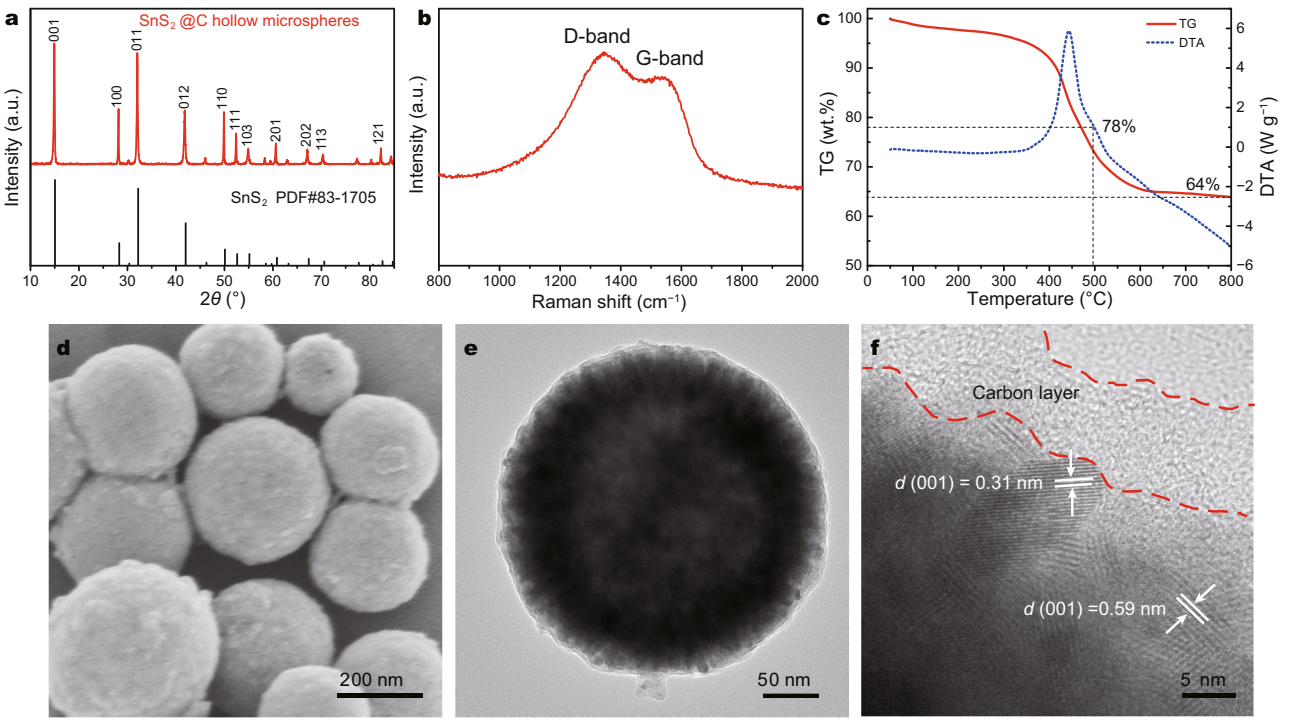

Figure 2 Characterizations of the SnS_2@C microspheres. (a) XRD patterns; (b) Raman curve; (c) TGA&DTA curves; SEM (d), TEM (e) and HR-TEM (f) images.

average thickness of ~10 nm (marked by red dashed line). Two typical lattice fringes were measured and their interplanar spacing are 0.31 and 0.59 nm, respectively, which are in good accordance to the planar distances of (100) and (001) for SnS_2, indicating the spheres are composed of polycrystalline grains with a high crystallinity. The TEM results again certify that the carbon layer was successfully coated onto the microspheres while the hollow structures from the SnO_2 have been entirely preserved.

Electrochemical performance

The electrochemical performances of the as-prepared SnS_2@C hollow microspheres are shown in Fig. 3. Fig. 3a displays the first three CV curves of the electrode within a voltage window of 0.01–3.0 V (*vs.* Li/Li^+) at a scan rate of 0.1 mV s^{-1}. Typically, four reduction peaks can be found in cathodic scans from the CV curves. The reduction peak at 1.83 V (*vs.* Li/Li^+) is known to arise from the lithium intercalation into SnS_2 without a phase decomposition (Equation (1)) [29,30]. The reduction peaks at 1.62 and 1.19 V (*vs.* Li/Li^+) in the first cathodic sweep could be attributed to the decomposition of SnS_2 into metallic tin and the formation of Li_2S (Equation (2)), which may occur in three steps [30], as well as the formation of a solid electrolyte interface (SEI) [11,31]. The peak at 0.22 V (*vs.* Li/Li^+) in the first anodic scan corresponds to the reversible formation of Li_xSn alloy (Equation (3)) and the oxidation peak at 0.50 V (*vs.* Li/Li^+) in the first anodic scan possibly originates from the delithiation reaction of Li_xSn alloy (Equation (3)). The above kinetics can be described by the electro-chemical conversion reactions [30,32]

$$SnS_2 + xLi^+ + xe^- \rightarrow Li_xSnS_2, \quad (1)$$

$$Li_xSnS_2 + (4-x)Li^+ + (4-x)e^- \rightarrow Sn + 2Li_2S, \quad (2)$$

$$Sn + 4.4Li^+ + 4.4e^- \rightarrow Li_{4.4}Sn. \quad (3)$$

The galvanostatic charge/discharge measurements of the SnS_2@C hollow microsphere anodes were performed within a voltage range of 0.01–3.0 V at a current density of 100 mA g^{-1} (Fig. 3b). The composite electrode delivers specific capacities of 1320 and 850 mA h g^{-1} for the first discharge and charge processes, respectively. The large initial capacity loss has led to a low coulombic efficiency of the first cycle (64%), which is attributed to the irreversible loss of Li ions resulting from the formation of an SEI layer on the electrode as well as partially irreversible decomposition of SnS_2 [33,34]. Although the first reversible discharge capacity decayed to 850 mA g^{-1}, the SnS_2@C hollow microsphere anode showed a con-

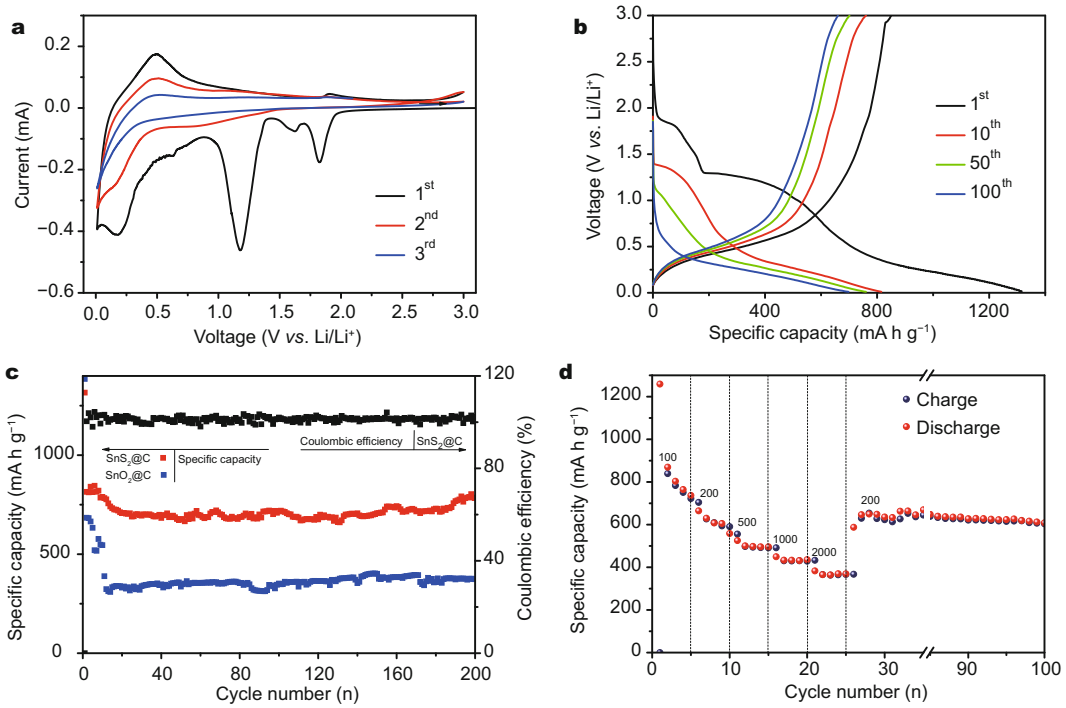

Figure 3 Electrochemical performances of the SnS_2@C and SnO_2@C hollow microsphere electrodes. (a) First three CV curves; (b) galvanostatic discharge/charge curves; cycling performances at a current density of 100 mA g^{-1} (c) and rate performances (d) of SnS_2@C.

siderably stable cycling performance after the first several cycles (Fig. 3c). The specific capacity remained at a very high value of 812 mA h g^{-1} after 200 cycles with a high capacity retention of 95.5% (Fig. 3c). Because the reversible capacity of SnS_2 is 645 mA h g^{-1} [10], and its irreversible capacity would gradually fade in the initial cycles, the extra capacity could be contributed by the carbon at about 170 mA h g^{-1}. The fluctuation of capacity during the cycle test could be possibly caused by the testing environment. The tiny fluctuation of temperature, humidity, and power supply may lead to the capacity fluctuations of the battery cells. Meanwhile, the cycle performance of SnO_2@C has been tested as a comparison (Fig. 3c). Although the first-discharge capacity is a little higher, it decreased to less than 400 mA h g^{-1} within the next 20 cycles, showing its worse performance than that of SnS_2@C. Compared to some of the previous work, the SnS_2@C reported in this work exhibited good electrochemical performance in specific capacities and cycle stability. For example, in a study by Luo *et al.* [35], the SnS_2-anode showed an initial discharge capacity as high as 1900 mA h g^{-1}, but the first reversible discharge capacity fell to 687 mA h g^{-1}. In another study by Yin *et al.* [36], the specific capacity of 913 mA h g^{-1} dropped to 547 mA h g^{-1} quickly after 50 cycles, although the first reversible discharge capacity was high.

Discharge/charge specific capacities of the SnS_2@C hollow microspheres at various current densities shown in Fig. 3d verifies their superior rate capability as anodes for LIBs. The specific discharge capacities are 780, 598, 500, 412 and 378 mA h g^{-1} at the current densities of 100, 200, 500, 1000 and 2000 mA g^{-1}, respectively. When the current rate was reset to 200 mA g^{-1}, a stable specific discharge capacity of approximately 606 mA h g^{-1} can be obtained. The capacity in the last 75 cycles is more stable than that at the same current rate of 200 mA g^{-1} in the 5–10th cycles. It may be due to the various irreversible processes at earlier working stage of battery. Capacity would gradually decrease under the synergistic effects of side reactions like the formation of SEI, irreversible phase change of SnS_2, and decomposition of electrolyte. Thus the capacity would become more stable when the side reactions come to a certain to reach an equilibrium. The good electrochemical performances at high current densities of these SnS_2@C hollow microsphere show their superiority over those previously reported SnS_2, such as graphene sheets-supported SnS_2 nanoplates in a study by Jiang *et al.* [37]. Therein the discharge capacity of the LIBs decayed from 642 to 240 mA g^{-1} when the current densities changed from 50 to 1000 mA g^{-1}. Three-di-

mensional SnS_2 hierarchitectures prepared by Wu *et al.* [38] demonstrated a discharge capacity of 706 mA h g^{-1} at 100 mA g^{-1} but decreased to 210 mA h g^{-1} at 1000 mA g^{-1}. As a whole, the above-discussed experimental results demonstrate good electrochemical properties of the SnS_2@C hollow microspheres. The superior LIBs performances of this electrode material can be explained as follows: (i) the hollow structures of the SnS_2@C could provide extra interior space to accommodate the volume expansion/contraction during the Li^+ insertion/extraction process [39]. (ii) The carbon shells prevented the restacking of SnS_2 microspheres or the crumbling of electrode material during continuous cycling [40]. (iii) The coated amorphous carbon in the composite can serve as the conductive species, which decrease the inner resistance of the LIBs, thus leading to a higher specific capacity and better rate capability [41].

CONCLUSIONS

In summary, hollow SnS_2 microspheres for LIBs anodes have been successfully synthesized by a facile method. The microspheres were completely protected by a layer of thin, conformal and self-supporting amorphous carbon shell. The rationally designed interior hollow allows a space for the expansion of SnS_2 without deforming the carbon shell. Owing to these unique structural features, the as-obtained SnS_2@C microspheres exhibit a very high reversible capacity of 850 mA h g^{-1} and reserve a value of 812 mA h g^{-1} after 200 cycles. Furthermore, they also show a superior rate capability. The results suggest their great potential as anode materials for the next-generation LIBs.

Received 29 June 2017; accepted 14 August 2017; published online 27 September 2017

1 Tarascon JM, Poizot P, Laruelle S, *et al.* Nano-sized transition-metal oxides as negative-electrode materials for lithium-ion batteries. Nature, 2000, 407: 496–499
2 Nam KT, Kim DW, Yoo PJ, *et al.* Virus-enabled synthesis and assembly of nanowires for lithium ion battery electrodes. Science, 2006, 312: 885–888
3 Lu Z, Wu X, Jiang M, *et al.* Transition metal oxides/hydroxides nanoarrays for aqueous electrochemical energy storage systems. Sci China Mater, 2014, 57: 59–69
4 Etacheri V, Marom R, Elazari R, *et al.* Challenges in the development of advanced Li-ion batteries: a review. Energ Environ Sci, 2011, 4: 3243
5 Pan A, Wang Y, Xu W, *et al.* High-performance anode based on porous Co_3O_4 nanodiscs. J Power Sources, 2014, 255: 125–129
6 Lou XW, Wang Y, Yuan C, *et al.* Template-free synthesis of SnO_2 hollow nanostructures with high lithium storage capacity. Adv Mater, 2006, 18: 2325–2329
7 Xu W, Xie Z, Cui X, *et al.* Hierarchical graphene-encapsulated hollow SnO_2@SnS_2 nanostructures with enhanced lithium storage capability. ACS Appl Mater Interfaces, 2015, 7: 22533–22541
8 Xu W, Zhao K, Niu C, *et al.* Heterogeneous branched core-shell SnO_2-PANI nanorod arrays with mechanical integrity and three dimentional electron transport for lithium batteries. Nano Energy, 2014, 8: 196–204
9 Sun Z, Liao T, Kou L. Strategies for designing metal oxide nanostructures. Sci China Mater, 2016, 60: 1–24
10 Seo J, Jang J, Park S, *et al.* Two-dimensional SnS_2 nanoplates with extraordinary high discharge capacity for lithium ion batteries. Adv Mater, 2008, 20: 4269–4273
11 Mei L, Xu C, Yang T, *et al.* Superior electrochemical performance of ultrasmall SnS_2 nanocrystals decorated on flexible RGO in lithium-ion batteries. J Mater Chem A, 2013, 1: 8658–8664
12 Zhai C, Du N, Yang HZD. Large-scale synthesis of ultrathin hexagonal tin disulfidenanosheets with highly reversible lithium storage. Chem Commun, 2011, 47: 1270–1272
13 Mukaibo H, Yoshizawa A, Momma T, *et al.* Particle size and performance of SnS_2 anodes for rechargeable lithium batteries. J Power Sources, 2003, 119-121: 60–63
14 Mahmood N, Hou Y. Electrode nanostructures in lithium-based batteries. Adv Sci, 2014, 1: 1400012
15 Lee KT, Jung YS, Oh SM. Synthesis of tin-encapsulated spherical hollow carbon for anode material in lithium secondary batteries. J Am Chem Soc, 2003, 125: 5652–5653
16 Xia H, Xiong W, Lim CK, *et al.* Hierarchical TiO_2-B nanowire@α-Fe_2O_3 nanothorn core-branch arrays as superior electrodes for lithium-ion microbatteries. Nano Res, 2014, 7: 1797–1808
17 Xia H, Xia Q, Lin B, *et al.* Self-standing porous $LiMn_2O_4$ nanowall arrays as promising cathodes for advanced 3D microbatteries and flexible lithium-ion batteries. Nano Energy, 2016, 22: 475–482
18 Ma J, Lei D, Duan X, *et al.* Designable fabrication of flower-like SnS_2 aggregates with excellent performance in lithium-ion batteries. RSC Adv, 2012, 2: 3615–3617
19 Xia J, Li G, Mao Y, *et al.* Hydrothermal growth of SnS_2 hollow spheres and their electrochemical properties. CrystEngComm, 2012, 14: 4279–4283
20 Wang J, Liu J, Xu H, *et al.* Gram-scale and template-free synthesis of ultralong tin disulfide nanobelts and their lithium ion storage performances. J Mater Chem A, 2013, 1: 1117–1122
21 Liu Y, Kang H, Jiao L, *et al.* Exfoliated-SnS_2 restacked on graphene as a high-capacity, high-rate, and long-cycle life anode for sodium ion batteries. Nanoscale, 2015, 7: 1325–1332
22 An C, Liu X, Gao Z, *et al.* Filling and unfilling carbon capsules with transition metal oxide nanoparticles for Li-ion hybrid supercapacitors: towards hundred grade energy density. Sci China Mater, 2017, 60: 217–227
23 Kong D, He H, Song Q, *et al.* A novel SnS_2@graphene nanocable network for high-performance lithium storage. RSC Adv, 2014, 4: 23372–23376
24 Liu J, Wen Y, van Aken PA, *et al. In situ* reduction and coating of SnS_2 nanobelts for free-standing SnS@polypyrrole-nanobelt/carbon-nanotube paper electrodes with superior Li-ion storage. J Mater Chem A, 2015, 3: 5259–5265
25 Wei Seh Z, Li W, Cha JJ, *et al.* Sulphur-TiO_2 yolk-shell nanoarchitecture with internal void space for long-cycle lithium-sulphur batteries. Nat Commun, 2013, 4: 1331
26 Nie Z, Wang Y, Zhang Y, *et al.* Multi-shelled α-Fe_2O_3 microspheres for high-rate supercapacitors. Sci China Mater, 2016, 59: 247–253

27 Qin L, Liang S, Pan A, *et al.* Zn_2SnO_4/carbon nanotubes composite with enhanced electrochemical performance as anode materials for lithium-ion batteries. Mater Lett, 2016, 164: 44–47
28 Qin L, Liang S, Tan X, *et al.* Zn_2SnO_4/graphene composites as anode materials for high performance lithium-ion batteries. J Alloys Compd, 2017, 692: 124–130
29 Zhuo L, Wu Y, Wang L, *et al.* One-step hydrothermal synthesis of SnS_2/graphene composites as anode material for highly efficient rechargeable lithium ion batteries. RSC Adv, 2012, 2: 5084–5087
30 Kim TJ, Kim C, Son D, *et al.* Novel SnS_2-nanosheet anodes for lithium-ion batteries. J Power Sources, 2007, 167: 529–535
31 Zhang Q, Li R, Zhang M, *et al.* SnS_2/reduced graphene oxide nanocomposites with superior lithium storage performance. Electrochim Acta, 2014, 115: 425–433
32 Wang G, Peng J, Zhang L, *et al.* Two-dimensional SnS_2@PANI nanoplates with high capacity and excellent stability for lithium-ion batteries. J Mater Chem A, 2015, 3: 3659–3666
33 Liu J, Wen Y, van Aken PA, *et al.* Facile synthesis of highly porous Ni-Sn intermetallic microcages with excellent electrochemical performance for lithium and sodium storage. Nano Lett, 2014, 14: 6387–6392
34 Liu J, Wen Y, Wang Y, *et al.* Carbon-encapsulated pyrite as stable and earth-abundant high energy cathode material for rechargeable lithium batteries. Adv Mater, 2014, 26: 6025–6030
35 Luo B, Fang Y, Wang B, *et al.* Two dimensional grapheme-SnS_2 hybrids with superior rate capability for lithium ion storage. Energy Environ Sci, 2012, 5: 5226–5230
36 Yin L, Chai S, Ma J, *et al.* Effects of binders on electrochemical properties of the SnS_2 nanostructured anode of the lithium-ion batteries. J Alloys Compd, 2017, 698: 828–834
37 Jiang X, Yang X, Zhu Y, *et al. In situ* assembly of graphene sheets-supported SnS_2 nanoplates into 3D macroporous aerogels for high-performance lithium ion batteries. J Power Sources, 2013, 237: 178–186
38 Wu Q, Jiao L, Du J, *et al.* One-pot synthesis of three-dimensional SnS_2 hierarchitectures as anode material for lithium-ion batteries. J Power Sources, 2013, 239: 89–93
39 Zeng L, Pan A, Liang S, *et al.* Novel synthesis of V_2O_5 hollow microspheres for lithium ion batteries. Sci China Mater, 2016, 59: 567–573
40 Wang YG, Wu W, Cheng L, *et al.* A polyaniline-intercalated layered manganese oxide nanocomposite prepared by an inorganic/organic interface reaction and its high electrochemical performance for Li storage. Adv Mater, 2008, 20: 2166–2170
41 Zheng L, Xu Y, Jin D, *et al.* Polyaniline-intercalated molybdenum oxide nanocomposites: simultaneous synthesis and their enhanced application for supercapacitor. Chem Asian J, 2011, 6: 1505–1514

Acknowledgements This work was supported by the National Natural Science Foundation of China (51302323), the Program for New Century Excellent Talents in University (NCET-13-0594), and the Innovation-driven Project of Central South University (2017CX001).

Author contributions Yang H and Su Y performed the experiments and wrote the article; Ding L participated in the experiments; Lin J performed the data analysis; Pan A and Zhu T proposed the experimental design. All authors contributed to the general discussion.

Conflict of interest The authors declare that they have no conflict of interest.

Hulin Yang is a postgraduate student in Prof. Pan's Group and will receive his Master degree from the School of Materials Science and Engineering at Central South University soon in 2018. His current research interest is tin-based materials for anode of lithium ion battery.

Anqiang Pan is currently a full professor at the School of Materials Science and Engineering, Central South University. His research interests focus on the synthesis of electrochemical energy storage materials and their applications, such as lithium ion batteries, supercapacitors and catalysts.

定向合成用于锂离子电池的高稳定性SnS_2@C空心微米球

杨岱林[1], 苏艳辉[1], 丁琳[1], 林建德[1], 朱挺[1*], 梁叔全[1], 潘安强[1*], 曹国忠[2]

摘要 锡基材料作为锂离子电池高容量负极材料得到了广泛研究. 然而循环充放电过程中的大体积变化通常会造成电极材料粉化. 本文报道了水热法合成SnO_2@C空心微米球, 再对其进行固相硫化制备SnS_2@C空心微米球的方法. 制得的SnS_2@C空心微米球具有独特的碳外壳及空心结构, 用作锂离子电池电极材料时, 在100 mA g^{-1}电流密度下表现出814 mA h g^{-1}的高可逆容量, 优秀的循环性能(循环200圈后仍保留783 mA h g^{-1}, 平均每圈损失0.02%), 以及出色的倍率容量(2 C时为433 mA h g^{-1}). 其内部空心部分可为充放电循环过程中的体积膨胀提供额外空间, 同时碳外壳能够保护微米球的完整性. 该SnS_2@C出色的电化学性能展示出用于下一代锂离子电池负极材料的应用前景.